

Supplementary Information

Unravelling steady-state bulk recombination dynamics in thick efficient vacuum-deposited perovskite solar cells by transient methods

David Kiermasch,^a Lidón Gil-Escrig,^{bc} Andreas Baumann,^d Henk J. Bolink,^b Vladimir Dyakonov,^{*ad}
and Kristofer Tvingstedt^{*a}

^a *Experimental Physics VI, Julius-Maximilian University of Würzburg, Am Hubland, 97074
Würzburg, Germany*

^b *Instituto de Ciencia Molecular, Universidad de Valencia, C/J. Beltrán 2, 46980, Paterna, Spain*

^c *Current address: Helmholtz-Zentrum Berlin für Materialien und Energie GmbH, Kekuléstraße 5,
12489 Berlin, Germany*

^d *Bavarian Center for Applied Energy Research, Magdalene-Schoch-Str. 3, 97074 Würzburg,
Germany*

Experimental Section

Materials for n-i-p devices: Photolithographically patterned ITO coated glass substrates were purchased from Naranjo Substrates. 2,2'-(Perfluoronaphthalene-2,6-diylidene)dimalononitrile (F6-TCNNQ), N4,N4,N4''-tetra([1,1'-biphenyl]-4-yl)[1,1':4',1''-terphenyl]-4,4''-diamine (TaTm) and N1,N4-bis(tri-p-tolylphosphoranylidene)benzene-1,4-diamine (PhIm) were provided from

Novald GmbH. Fullerene (C_{60}) was purchased from Sigma Aldrich. PbI_2 was purchased from Tokyo Chemical Industry CO (TCI), and CH_3NH_3I (MAI) from Lumtec.

Preparation of the n-i-p devices: ITO-coated glass substrates were subsequently cleaned with soap, water and isopropanol in an ultrasonic bath, followed by UV-ozone treatment. They were transferred to a vacuum chamber integrated into a nitrogen-filled glovebox (MBraun, H_2O and $O_2 < 0.1\text{ppm}$) and evacuated to a pressure of $1 \cdot 10^{-6}$ mbar. The vacuum chamber is equipped with six temperature-controlled evaporation sources (Creaphys) fitted with ceramic crucibles. The sources were directed upwards with an angle of approximately 90° with respect to the bottom of the evaporator. The substrate holder to evaporation sources distance is approximately 20 cm. Three quartz crystal microbalance (QCM) sensors are used, two monitoring the deposition rate of each evaporation source and a third one close to the substrate holder monitoring the total deposition rate. For thickness calibration, we first individually sublimed the charge transport materials and their dopants (TaTm and F6-TCNNQ, C_{60} and PhIm). A calibration factor was obtained by comparing the thickness inferred from the QCM sensors with that measured with a mechanical profilometer (Ambios XP1). Then these materials were co-sublimed at temperatures ranging from 135-160 °C for the dopants to 250 °C for the pure charge transport molecules, and the evaporation rates were controlled by separate QCM sensors and adjusted to obtain the desired doping concentration. In general, the deposition rate for TaTm and C_{60} was kept constant at 0.8 \AA/s while varying the deposition rate of the dopants during co-deposition. Pure TaTm and C_{60} layers were deposited at a rate of 0.5 \AA/s . For this n-i-p configuration, 40 nm of the n-doped electron-transport layer (n-ETL, C_{60} :PhIm) capped with 10nm of the pure C_{60} were deposited. Once completed this deposition, the chamber was vented with dry N_2 to replace the

–ETL crucibles with those containing the starting materials for the perovskite deposition, PbI_2 and $\text{CH}_3\text{NH}_3\text{I}$. The vacuum chamber was evacuated again to a pressure of 10^{-6} and the perovskite films were then obtained by co-deposition of the two precursors. The calibration of the deposition rate for the $\text{CH}_3\text{NH}_3\text{I}$ was found to be difficult due to non-uniform layers and the soft nature of the materials which impede accurate thickness measurements. Hence, during the evaporation the rate of the $\text{CH}_3\text{NH}_3\text{I}$ was kept at 1 \AA/s and the rate of the PbI_2 was kept at 0.5 \AA/s . These rates were adjusted by grazing incident x-ray diffraction. After deposition of the perovskite film, the chamber was vented, and the crucibles replaced with those containing TaTm and F6-TCNNQ and evacuated again to a pressure of 10^{-6} mbar. The devices were completed depositing a film of pure TaTm and one of the p-HTL (TaTm: F₆-TCNNQ), with a thickness of 10 and 40 nm, respectively. Finally, the substrates were transferred to a second vacuum chamber where the metal top contact (100 nm thick) was deposited.

Preparation of PEDOT:PSS device: Solar cells are fabricated on ITO covered glass substrates. Poly(3,4-ethylenedioxythiophene):poly(styrenesulfonate) (PEDOT:PSS) was spin coated to form a hole transport layer with a thickness of around 40 nm. Perovskite films were synthesized with the well-known two-step interdiffusion process using PbI_2 (400mg/ml) dissolved in N,N-Dimethylformamide and $\text{CH}_3\text{NH}_3\text{I}$ (40mg/ml) dissolved in 2-Propanol. After spin-coating the PbI_2 -solution, the substrate was annealed for 15 minutes at 70 °C. Afterwards, MAI was spin-coated, and the substrates were heated at 100 °C for 90 minutes to form the active layer (around 350 nm). In the next step, PC₆₀BM was spin casted from 1,2-Dichlorobenzene solution with a concentration of 20 mg/ml followed by 60 minutes of annealing at 100°C. Finally, the substrates

were transferred into an evaporation chamber to apply C₆₀, Bathocuproin (BCP) and gold (Au) layers.

Current-voltage characterization and transient measurements: Current–voltage characterization was performed under inert atmosphere using a Keithley 2612 source measure unit (SMU) and an AM1.5G solar simulator (LOT-Oriel) which is calibrated to 100 mW/cm² (1 sun). The scan-speed was kept at 100 mV/s for all measurements.

Transient photovoltage (TPV) measurements were realized in a closed helium contact gas cryostat without exposure to ambient air using a 10W white light LED for bias light illumination. To vary the background illumination intensity over five order of magnitudes (10⁻⁵ suns – 3 suns) the LED current was controlled in combination with different neutral density filters. 1 sun equivalent was defined by the LED current matching the same short circuit current density J_{sc} of a solar cell as measured previously with the sun simulator. The solar cells were kept under open-circuit conditions using a 1 G Ω input impedance amplifier. A pulsed Nd:YAG laser ($\lambda = 532$ nm excitation pulse, 80 ps) is providing a small optical perturbation generating additional charge carriers in the device. The voltage transient was then recorded by a digital storage oscilloscope (Agilent Infinium DSO90254A) and fitted with both a single and double exponential function. Charge carrier extraction (CE) measurements were performed in the same cryostat directly after TPV. The premeasured open-circuit voltage (using a Keithley 2602) is measured in the cryostat for every light intensity and applied to the solar cell under constant LED illumination. Triggered by the double pulse generator (Agilent 81150A), the LED was switched off by shortening the voltage source (Keithley 2602) with a high-power transistor. The resulting current transient was monitored via the digital storage oscilloscope mentioned above. The integrated charge was then

corrected by capacitive charge carriers. For this, measurements in the dark at low negative voltages (-0.35 V - -0.05 V) are conducted, where the charges which are stored on the device electrodes are extracted.

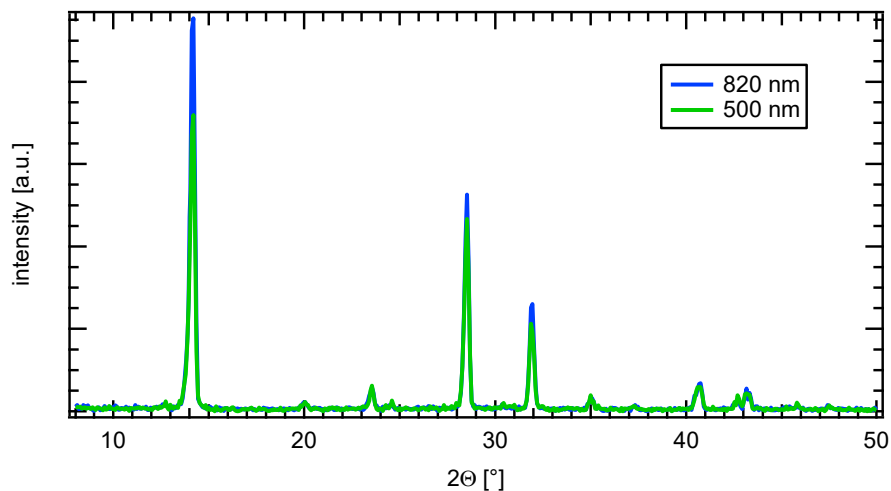


Figure S1. Grazing incidence X-ray diffraction pattern from 500 nm and 820 nm co-evaporated MAPbI₃ films. The crystallinity is similar for both film thicknesses.

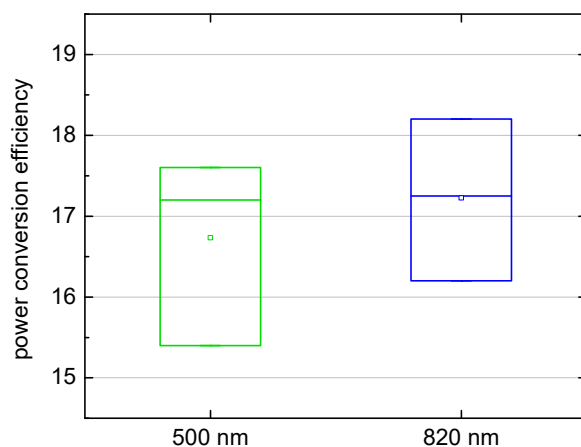


Figure S2. Box charts for power conversion efficiency of both studied device thicknesses. Slightly higher power conversion efficiencies are obtained for the thicker devices as the absorption increases as discussed in the main manuscript.

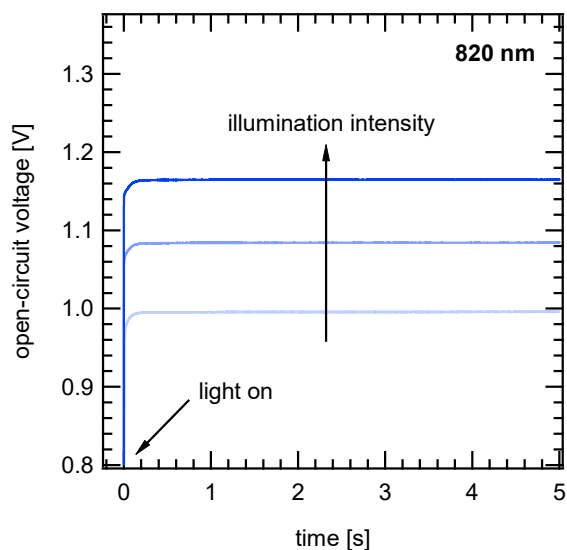


Figure S3. Evolution of open-circuit voltage for the 820 nm device after switching on the light for three different light intensities. Independent of illumination intensity, the V_{OC} reaches a plateau within the first few hundred milliseconds.

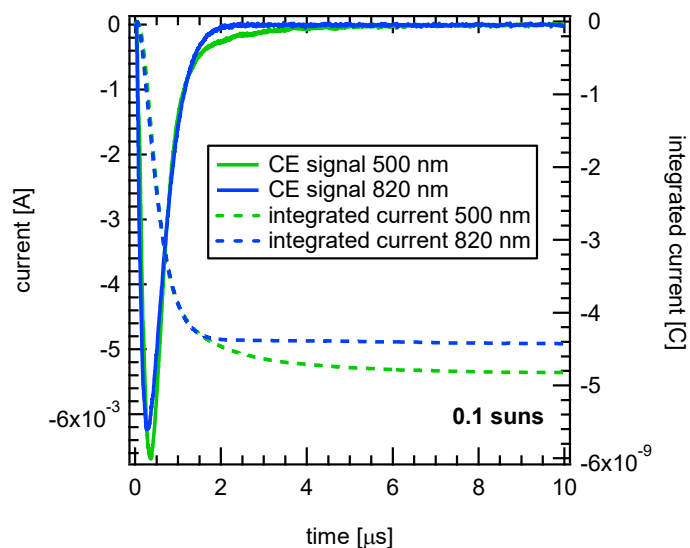


Figure S4. Raw charge extraction signals (solid lines, left y-axis) and the integral (dashed lines, right y-axis) for both 500 nm and 820 nm devices measured under 0.1 sun illumination conditions. A fast charge extraction pulse within a few hundred nanoseconds can be observed for both devices.

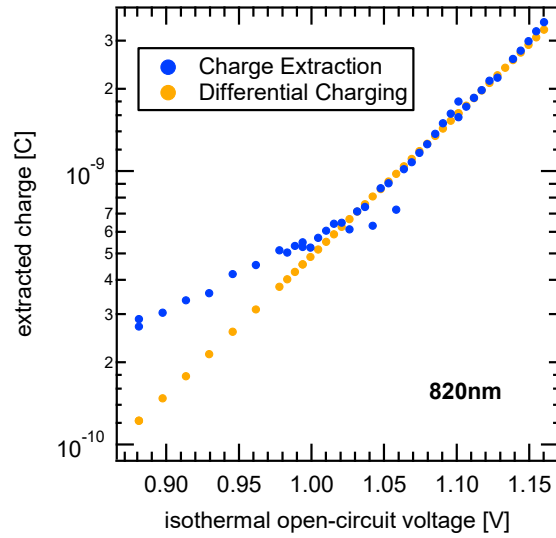


Figure S5. Comparison of Charge Extraction and Differential Charging. In the high voltage regime (bulk charge carriers) both methods provide the same amount of extracted charge, while the difference at lower voltages originates from the different methods to account for device capacitance.

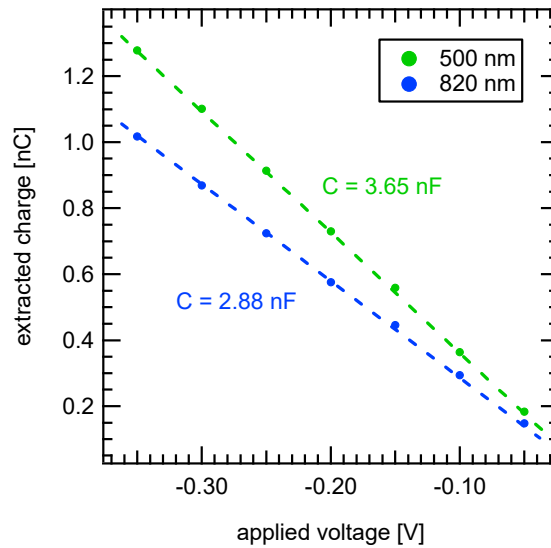


Figure S6. Extracted charge from charge extraction experiments without illumination under negative voltages in the range of -0.05 V down to -0.35 V. From a linear fit, a capacitance of 3.65 nF for the 500 nm solar cell and 2.88 nF for the 820 nm device can be obtained.

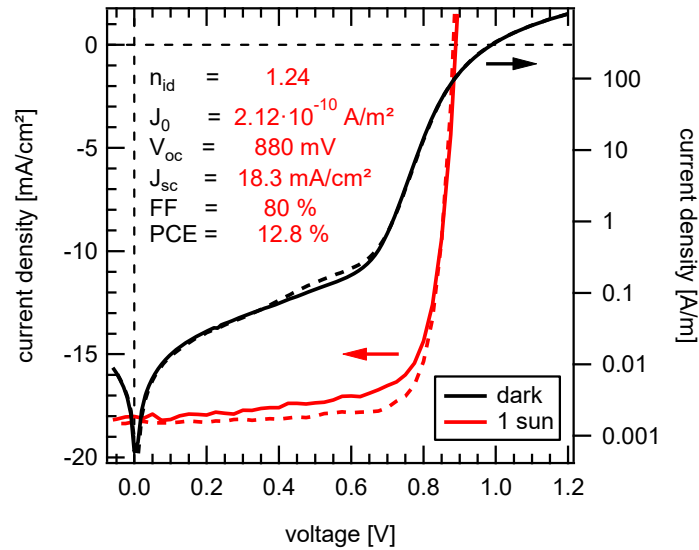


Figure S7. Illuminated (left y-axis) and dark (right y-axis) j-V curves of a 350 nm solution-processed perovskite device with PEDOT:PSS as a hole transport layer and C₆₀, PC₆₀BM and BCP as electron transport layers.

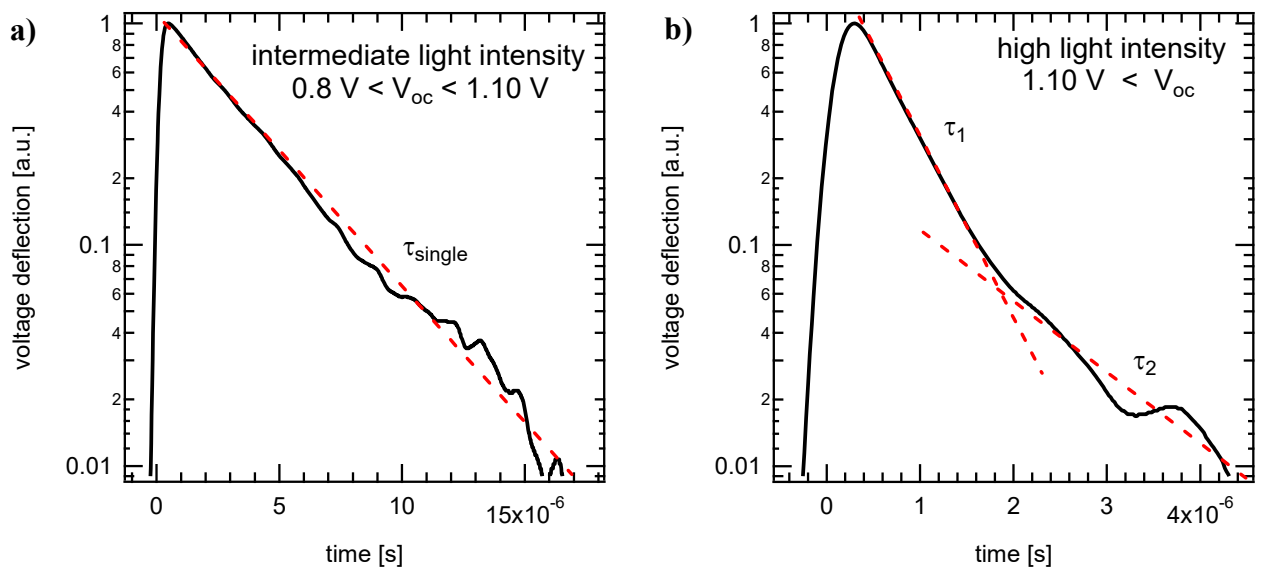


Figure S8. Two examples of raw transient photovoltage signals for two different illumination intensities (open circuit voltages): **a)** In case of intermediate light intensities ($0.80 \text{ V} < V_{oc} < 1.10 \text{ V}$) a single exponential decay is observed. **b)** For high light intensities with open circuit voltages higher than 1.10 V the decay could be better described with two lifetimes τ_1 and τ_2 .